Design of a passive alternative for long stroke linear aerostatic stages based on ferrofluid bearings

van den Toorn, Stefan W.M.; Spronck, Jo W.; van Ostayen, Ron A.J.; Lampaert, Stefan G.E.

DOI
10.1016/j.precisioneng.2020.09.021

Publication date
2021

Document Version
Final published version

Published in
Precision Engineering

Precision Engineering 67 (2021) 428–437

Contents lists available at ScienceDirect

Precision Engineering

journal homepage: www.elsevier.com/locate/precision

Design of a passive alternative for long stroke linear aerostatic stages based on ferrofluid bearings

Stefan W.M. van den Toorn, Jo W. Spronck, Ron A.J. van Ostayen, Stefan G.E. Lampaert *

Department of Precision and Microsystems Engineering, Delft University of Technology, Delft, The Netherlands

ARTICLE INFO

Keywords:
Magnetic fluid
Passive bearing
Ferrofluid linear stage
Air bearing alternative
Ferrofluid design

ABSTRACT

The objective of this research is to demonstrate the capability of a long stroke linear ferrofluid (FF) stage. This stage is a passive alternative to existing linear aerostatic stages and can be used in low loaded CNC devices, pick and place machines, microscopy or scanner applications. To compete with aerostatic stages the bearing must be repeatable and achieve sufficient stiffness for the application. The effects of ferrofluid trail formation are countered with the use of a ferrofluid reservoir located on the mover. To increase stiffness a specially designed magnet configuration is used. A linear guidance was built with outer dimensions of 180x600x80 mm (WxLxH), a mover of 1.8 kg without actuator and payload having a 430 mm stroke. The load capacity of the stage was measured to be 120 N, with a stiffness of 0.4 N/μm. The maximum height delta after a stroke with 1 kg payload and a mover velocity of 0.25 m/s was measured to be less than ±3 μm, and with 1.75 kg payload and a velocity of 0.5 m/s the height delta was within ±7 μm. Using a rheometer, it was shown that the effects of evaporation in ferrofluid can be reversed, within certain limits of mass loss, by adding carrier fluid. The damping is shown to be a function of payload and velocity and was measured to be between 2 and 4 N·s/m for velocities between 0.2 and 0.5 m/s. In comparison to a linear aerostatic stage it can be concluded that while the linear ferrofluid stage is outperformed in stiffness and out-of-plane repeatability, the ferrofluid stage does not require a continuous supply of air and has lower fabrication tolerances due to the higher fly height. Thus, the linear ferrofluid stage is a cost-effective alternative to a linear aerostatic stage when the stiffness and straightness are of less importance.

1. Introduction

The aerostatic bearing cannot be overlooked in current precision positioning systems. The relatively simple concept of floating on top of a cushion of air has obtained a major market share in the past decades [1]. The use of pressurized air however also has its downside, as the bearing seizes when the air pressure is stopped, the manufacturing tolerances are very tight and the low damping gives problems in controlling the movement [2]. In the search for alternatives we find that conventional bearings such as ball or journal bearings suffer from stick–slip, magnetic bearings suffer from complexity and flexures suffer from energy storage and a limited range of motion. A bearing type free from all of these issues is the ferrofluid bearing.

The ferrofluid bearing consists of a ferrofluid in between bearing surfaces in a magnetic field. Ferrofluid is a stable colloidal suspension of magnetic particles (diameter ~10 nm) in a carrier fluid [3]. The bearing itself relies on pressure build-up in the fluid as it is attracted by a magnetic field. This pressure build-up is caused by the displacement of the fluid from a position with a high magnetic field to a position with a lower magnetic field. This generates a normal force onto the bearing surface. Alternatively, the ferrofluid can be used to seal a pressurized pocket of air which provides the normal force. The first concept is known as the ferrofluid pressure bearing [4], the second is known as the ferrofluid pocket bearing [5]. The working principle of these bearings is illustrated in Fig. 1.

The relation between the ferrofluid bearing and other bearing solutions can be seen in Table 1. The table shows that the aerostatic bearing outperforms the ferrofluid bearing in load capacity and stiffness. However, the ferrofluid bearing can fill a niche that has been left by the other bearing types i.e. low-cost passive applications requiring a smooth motion without demand for high stiffness in constrained directions. These applications can range from low loaded CNC devices such as 3D printers or laser cutters to optical devices such as microscopy or scanners. An entirely different field of application would be the use in zero gravity environments, as the fluid can be contained in the magnetic field.

* Corresponding author.
E-mail address: s.g.e.lampaert@tudelft.nl (S.G.E. Lampaert).

https://doi.org/10.1016/j.precisioneng.2020.09.021
Received 12 February 2020; Received in revised form 19 August 2020; Accepted 26 September 2020
Available online 13 October 2020

Table 1
An indication of the performance of ferrofluid bearings in comparison to other bearing solutions for precision positioning [6–10]. The ferrofluid bearing is taken as benchmark, a better performance in precision positioning applications is denoted with +. Performance in load capacity and stiffness is evaluated considering the constrained directions.

	Ferrofluid	Active magnetic	Hydrostatic	Aerostatic	Roller bearing
Load capacity	0	+	+ +	0	+
Stiffness	0	+ +	+ +	+	+ +
Static friction	0	0	0	0	– –
Dynamic friction	0	– –	0	– –	–
Surface finish requirement	0	+ +	–	– –	– –
Complexity	0	– –	–	–	0
Advantage	No stick slip	UH vacuum compatible	Large loads	Contactless	Standardized
Disadvantage	Low stiffness	Inherently unstable	Lubrication oil	Supply Pressure	Stick–slip

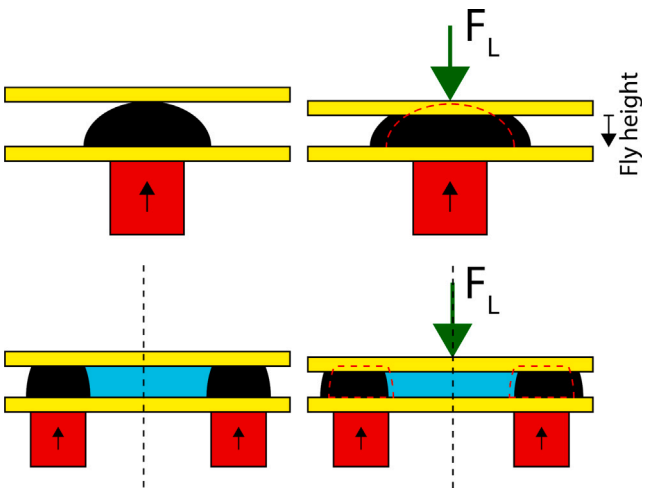

Fig. 1. Working principle pressure bearing (up) and pocket bearing (down).

The ferrofluid bearing has some other advantages. When a Lorentz type actuator is used, the magnetic field to activate the ferrofluid is already available. The system only requires low tolerances on surface waviness and smoothness compared to similar high precision bearings due to the large (~0.5 mm) distance between bearing surfaces. The ferrofluid itself acts as a lubricant. The large surface area in contact with the fluid allows for heat transfer between the bearing surfaces. The broad choice in carrier fluid makes it possible to tune the bearing for different environments, for example a fluid with a low vapour pressure for use in a vacuum, or a fluid with a low viscosity for fast motion. The amount of physical damping makes controlling the system easier. It decreases the sensitivity to high frequency disturbances, thus reducing the need for complicated filtering [11–14] or external damping [15,16].

In the last decade ferrofluid bearings have been implemented into various planar positioning systems [17–22] and into linear stages [23–25], the behaviour in load capacity and damping has been studied [26–32], and finally basic design rules for ferrofluid bearings have been formulated by Lampaert [33]. Still all existing demonstrators suffer from low repeatability in the constrained directions and possess a limited range of motion. These issues are the result of the loss of encapsulated air from the pocket in pocket bearings and the loss of ferrofluid due to trail formation.

In this study a passive long stroke linear stage based on ferrofluids is proposed. The challenges in the long stroke bearing primarily are to achieve sufficient stiffness, repeatability and stroke length. Problems and implementations of the solutions are discussed, designed and build in a demonstrator stage for the purpose of verification. The specifications for this demonstrator stage are based on those of a commercially available aerostatic linear stage.

2. Stage design and modelling

The proposed demonstrator is based on an existing linear bearing stage from Physical Instrumente, the A-110. This air bearing stage is marketed as an affordable high performance nanopositioning stage. The aim of the demonstrator stage is to be interchangeable with this aerostatic stage, thus conforming to the same or better specifications. These specifications can be seen in Table 2.

2.1. Challenges

In the design of the stage some specific challenges are considered. The most pressing matters are air loss from the encapsulated pocket of air, ferrofluid trail formation and evaporation. Air loss is distinctive for ferrofluid pocket bearings, where the fly height is permanently reduced once the bearing is loaded beyond the load capacity of the ferrofluid seal. The fly height is defined as the distance between bearing surfaces and can be seen in Fig. 1. Trail formation is the occurrence of fluid being left behind as the bearing is translated. Evaporation changes the composition of the ferrofluid suspension and alters the fluid properties such as viscosity and saturation magnetization. If left unaddressed, each problem can severely compromise the performance and repeatability of the stage. Solutions for each of these problems have been implemented in the demonstrator stage.

The problem of air loss is distinctive for ferrofluid pocket bearings only, the ferrofluid pressure bearing does not suffer from this problem. In terms of load capacity and stiffness, the pocket bearing outperforms the pressure bearing [30,32]. For the selected application, the repeatability of the bearing motion is considered more desirable than load capacity or stiffness, and therefore the pressure bearing is the preferred bearing type for this application.

The trail formation problem is solved by the creation of a reservoir on the mover itself. By assuming a Couette flow between the bearings and base the total amount of fluid loss for a stroke of 300 mm is estimated at 20 ml. In a subsequent stroke the same 20 ml of fluid is lost again, however, the magnets will also move over the previously lost fluid and recollect it. Thus, this 20 ml is the total volume of ferrofluid in the trail during operation. As the volume of fluid required is low compared to the volume of the mover, it is feasible to place additional ferrofluid on the mover. This reservoir is created by placing the top, bottom and side bearing pads close together, as can be seen in Fig. 2. The high magnetic field at the corners ensures there is a supply of ferrofluid on the mover. As there is no contact between the ferrofluid in the reservoir and the base, it is not contributing to the load capacity. The high magnetic field also ensures ferrofluid can move freely between the individual pressure bearings. This ensures a repeatable behaviour and redistribution of the ferrofluid collected from the previous trail.

The design of the stage is a double U shape as shown in Fig. 2. The top bearing pad produces a preload which increases the stiffness and the symmetric design reduces tilt under acceleration and deceleration. The in-plane length of the mover is 100 mm, to save weight and to reduce damping. The areas marked in red are reserved for 6 bearing pads, two of 50 × 100 × 4 mm (W × L × H) for the bottom bearings and

Table 2
Specifications of A-110.300 linear air bearing stage [34].

Model	A-110.300
Travel	300 mm
Maximum payload	10 kg normal
Flatness	< ± 2 μm
Moving mass	2.6 kg
Maximum velocity	1 m/s
Outer dimensions	160 × 575 × 60 mm (W × L × H)
Mover dimensions	160 × 200 × 60 mm (W × L × H)

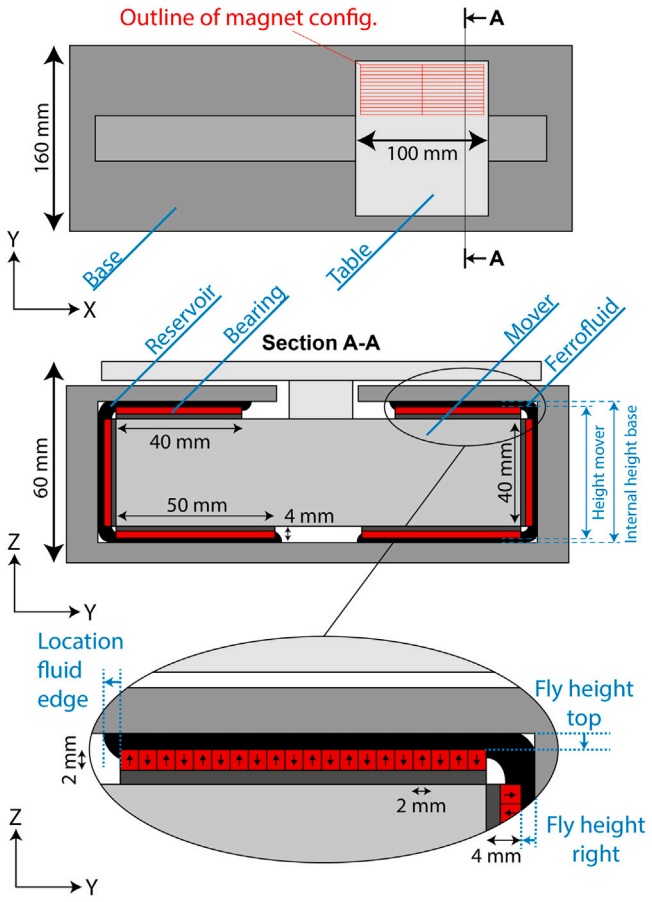

Fig. 2. Schematic bearing design with areas reserved for bearing in red. (For interpretation of the references to colour in this figure legend, the reader is referred to the web version of this article.)

four 40 × 100 × 4 mm (W × L × H) for the side and top bearings. Each bearing pad consists of 50 × 2 × 2 mm magnets from HKCM [35]. These magnets are arranged in an 'up–down' magnetization configuration with the long side in the x-direction as can be seen in Fig. 2. The bottom bearing pads consist of a 2 × 25 grid (x ∗ y), the top and side bearing pads are slightly smaller and consist of a 2 × 20 grid (x ∗ y). The outline of the top bearing pad is indicated in Fig. 2. The use of many small magnets results in a concentrated magnetic field close to the magnets with a large gradient in the direction of the fly height. This in turn results in a high load capacity and stiffness for the ferrofluid pressure bearing. Instead of an up–down magnetization configuration, the magnets could also be magnetized facing each other, all in the same direction or with the direction oriented in a Halbach array. Alternatively, also iron can be used in between the magnets to shape the magnetic field. It was found that from these possible configurations the up–down configuration with an iron bottom plate is the most cost-effective way to achieve a high stiffness and load capacity while also having little moving mass [36]. A second benefit of this arrangement is the low stray field, as the field of individual magnets is cancelled at larger distances. Magnets with a smaller cross-section can further increase the stiffness of the bearing, but the brittleness and increased number of magnets would make assembly complex. Ferritic stainless steel is used instead of iron to eliminate the risk of oxidation. Although 0.5 mm thickness of the bottom plate would already have yielded the same performance, for assembly purposes a relative thick bottom plate of 2 mm has been used. As the pressure bearings are located close together, the magnetic field intensity is relatively high at adjacent corners of the bearing pad as can be seen in Fig. 2. The ferrofluid that accumulates there has a negligible effect on the load capacity of the stage, and this is used as a reservoir of ferrofluid to counter the effects of trail formation. As this reservoir bridges the different bearing pads it also can transport fluid between the bearing pads, ensuring a repeatable performance.

For this research the kerosene based EFH3 fluid from Ferrotec has been chosen. The reason for this choice it the relatively high saturation magnetization of 66 mT and low viscosity of 12 mPa s [37] in comparison to other ferrofluids. The high saturation magnetization increases load capacity and stiffness of the stage [32]. The low viscosity of the ferrofluid reduces the overall damping in the stage [31]. As this fluid has a non-negligible vapour pressure the evaporation of the ferrofluid needs to be addressed. In order to do this, a method to resupply the evaporated carrier fluid has been researched as well.

2.2. Modelling stage load capacity and stiffness

Using a two dimensional numerical model of the magnetic field in COMSOL [38] and Matlab [39], the load capacity and stiffness of the bearing pads were determined. The geometry of the pad was defined in Matlab using the COMSOL Livelink interface, the magnetic field was then calculated in COMSOL using the Magnetic Fields, No Currents interface (mfnc) in the AC/DC module. Using the modelled magnetic field and Eqs. (1) and (2) the respective load capacity and stiffness of the magnet configuration were modelled.

$$F_L = \mu_0 M_s \int_S H\,dA \tag{1}$$

$$k = -\mu_0 M_s \frac{d}{dh} \int_S H\,dA \tag{2}$$

In these equations F_L is the load capacity, μ_0 the permeability in vacuum, M_s the saturation magnetization of the ferrofluid and H the magnetic field intensity. The area is defined as the surface area of the ferrofluid on the top bearing surface, and this is dependent on the location of the outer fluid edge and the length of the magnet configuration.

In the model several assumptions are made, for the remanent flux density of the magnets (1.17 T), saturation magnetization of the ferrofluid (66 mT), and for the location of the fluid edge (5 mm). The definition of the fluid edge location is shown in Fig. 2. The ferrofluid itself is has a relative permeability of 1. For the ferritic stainless steel, a relative permeability of 4000 is used with a saturation magnetization of 1.4 T.

The preload generated by the top bearing pads can be varied by modifying the difference in height of the mover and the internal height of the base as can be seen in Fig. 2. The design of the demonstrator is made such that this height difference can be modified easily. Decreasing the height difference decreases the fly height of the top and bottom bearing pads and thus increases the applied preload. As the ferrofluid bearing can be seen as a mechanical spring this increases the stiffness of the bearing. The increased stiffness however comes at the cost of less load capacity and more viscous damping. Decreasing the fly height also reduced the amount of fluid necessary as the physical volume between the bearing surfaces decreases. An additional effect of the preload is a more stable fly height as the trail formation will also occur on the top side and thus, the fluid loss is symmetrical. As the bearing pads on top

Table 3
Bearing characteristics in horizontal and vertical plane for different fly heights. Stiffness is evaluated around equilibrium position. Load capacity is evaluated at the minimum fly height of 0.1 mm.

Horizontal			
Fly height left pad [mm]	Fly height right pad [mm]	Load [N]	Stiffness [N/μm]
0.1	1.9	120	0.23
0.1	0.9	92	0.27
0.1	0.4	49	0.34
0.1	0.15	11	0.43
Vertical			
Fly height bottom pad [mm]	Fly height top pad [mm]	Load [N]	Stiffness [N/μm]
0.1	0.9	231	0.68
0.1	0.4	146	0.81
0.1	0.15	69	0.97

Table 4
Simulation of eddy current damping in full size pressure bearing pad. Magnet dimensions 50 × 2 × 2 mm, arranged in a 2 ∗ 25 (x ∗ y) grid with long edge in x-direction, magnetized alternating between positive and negative z-direction.

Fly height [mm]	Eddy current damping coefficient [N s/m]
0.10	0.22
0.25	0.13
0.50	0.07
1.00	0.03

and bottom differ in size and gravity acts on the mover, the equilibrium fly height of the top and bottom pad will not be exactly the same.

Table 3 shows the bearing characteristics as a function of the fly height according to the model. In order to achieve the same specifications as the A-110 aerostatic stage the fly height in vertical direction will need to be somewhere between 0.5 mm and 0.25 mm. As no horizontal payload is specified for this aerostatic stage the fly height of the horizontal pads is set to 1 mm each.

2.3. Eddy current damping in stage

Aluminium is the preferred material for the demonstrator stage due to its availability and machinability. The relative velocity between the highly conductive aluminium and the magnetic fields induced by the bearing pads will create eddy currents. The damping induced by these eddy currents is investigated using a COMSOL model. This modelling is done in three dimensions using the mfnc interface in the AC/DC module. Fig. 3 illustrates this model and the direction of the relative velocity between the bearing pad and conductor. In the model the bearing pad is translated past a aluminium block (infinite length, 20 mm height), this is modelled using the Lorentz term velocity in the mfnc interface. The bearing pad consists of 2 × 25 magnets (x ∗ y) of 50 × 2 × 2 mm with a remanent flux density of 1.17 T. The results of the modelling can be seen in Table 4.

In Table 4 it can be seen that the simulated eddy current damping is low. The low damping is caused by two factors. Firstly, as eddy currents are induced by a change in magnetic field the current loops only occur at the start and end of the bearing pad. Secondly, as the magnetization direction of the magnets alternate the direction of the current alternates as well. This prevents large current loops from forming. Both factors can be seen in Fig. 3.

3. Methods for design validation

To verify that the functioning of the stage is as intended, first the load capacity and stiffness model of an individual pressure bearing pad are validated. This same model is used in the verification of the load and stiffness of the full stage. To gain insight in the performance of the stage when in use, the effects of trail formation and evaporation will be measured. Finally, the damping in motion direction will be experimentally determined. This understanding of the damping will be useful in the future actuation and control of the stage.

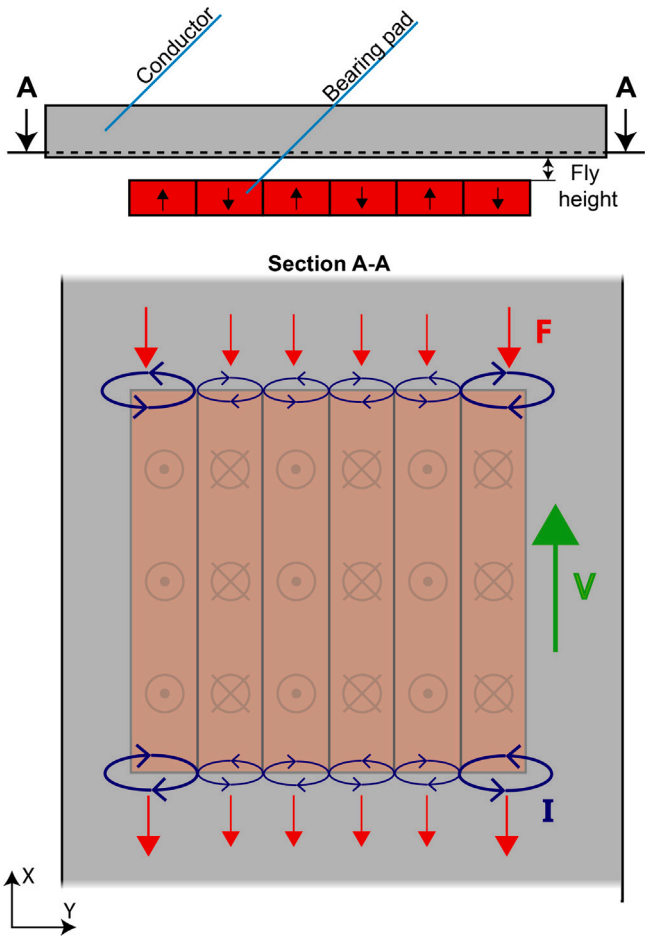

Fig. 3. Illustration of the location and magnitude of the eddy currents (I) on the surface of the conductor. With the direction of the relative velocity between conductor and bearing pad (V) in green and damping force (F) direction in red. (For interpretation of the references to colour in this figure legend, the reader is referred to the web version of this article.)

3.1. Single pressure bearing pad

The individual tested pressure bearing pad is assembled of 23 50 × 2 × 2 magnets [35] with a remanent flux density of 1.17 T structured as seen in Fig. 2. The pad is tested with 5 ml of EFH3 fluid and with the same amount of APG 513A ferrofluid. The load–fly height curve of the bearing is modelled and measured in a compression test using a Zwick/Roell Z005 materials test frame.

For the modelling of the pressure bearing path the location of the outer fluid edge is needed. This variable is defined in Fig. 2, and represents the starting point of the pressure build-up in the fluid. The location is primarily dictated by the equilibrium between the gravitational pull and the magnetic body force on the fluid. Using the Mfnc interface in the AC/DC module in COMSOL a two dimensional model of the magnetic field surrounding the bearing pad is simulated. The results of this simulation can be seen in Fig. 4. It was found that the magnetic field further than 0.9 mm outside the magnet was too weak to overcome the gravitational pull on the fluid. The effect of surface tension and surface roughness on this location is assumed to be negligible compared to the magnetic body force in this calculation. The

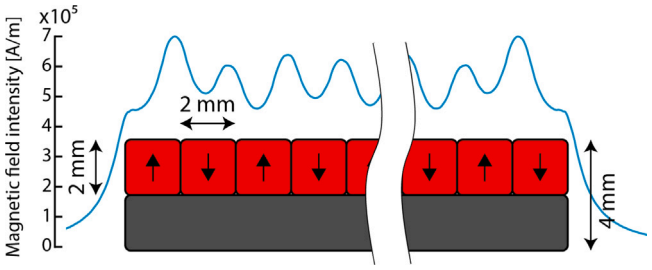

Fig. 4. Modelling of magnetic field surrounding ferrofluid pressure bearing pad.

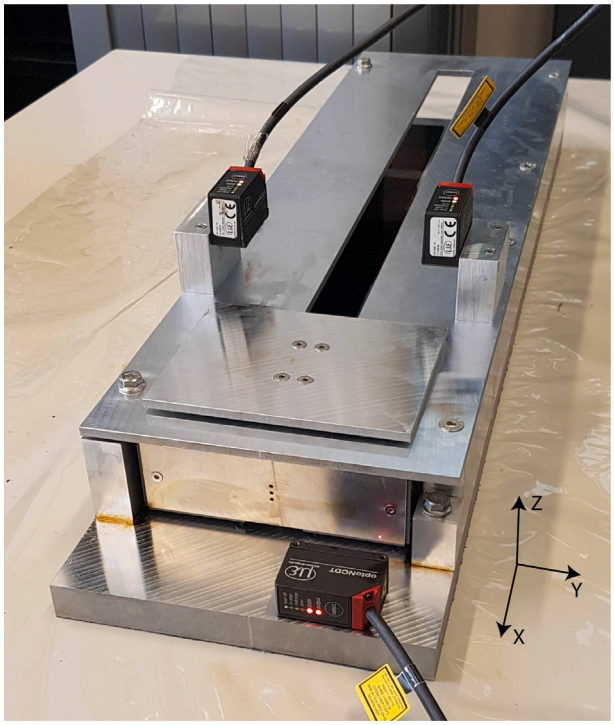

Fig. 5. Measurement setup of demonstrator with 3 laser distance sensors for position and roll of the mover.

Table 5
Physical properties of realized demonstrator stage.

Travel	460 mm
Moving mass	1.84 kg
Outer dimensions	180 × 640 × 80 mm (W × L × H)
Mover dimensions	139 × 124 × 60 mm (W × L × H)

magnetization saturation of the ferrofluid is modelled as 32 kA/m [40] for the APG 513A and 52.5 kA/m for the EFH3 [41].

3.2. Demonstrator stage

The demonstrator as seen in Fig. 5 was constructed from aluminium with ferritic stainless-steel bottom plates for mounting the magnets. The top plate could be raised using shims to increase the fly height of the top and bottom bearing pads. The total material cost for the ferrofluid demonstrator stage are slightly over €1000, the magnets contribute €150 of the total cost.

In Table 5 the physical properties of the realized stage can be seen. The base and mover have both been over-designed. Thicker metal is used in order to increase production efficiency and to allow for more freedom in the fine-tuning of the height difference between mover and base. Because of this, if useful, the width and height of the outer dimensions could both be reduced with 20 mm without any performance loss.

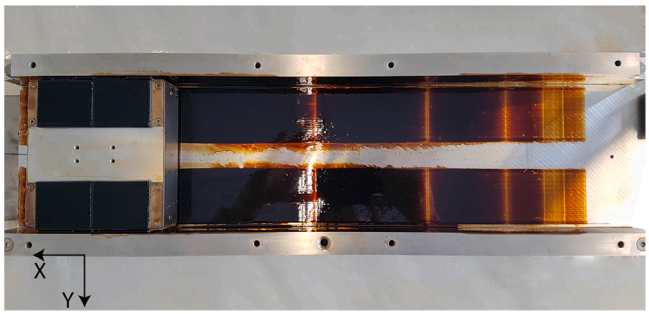

Fig. 6. Trail formation in stage. The mover has been displaced in steps increasing in velocity from right to left. The table and top plate were removed before the displacement.

Fig. 5 shows the demonstrator and the three Micro-Epsilon optoNCDT 1420 laser distance sensors [42] used. 2 sensors with a range of 10 mm were fitted above the table on either side. These sensors measure the position of the table relative to a fixed frame. From this the fly height and roll of the stage could be found. One sensor with a range of 200 mm was mounted in front of the mover and was used to measure displacement and velocity of mover. The demonstrator stage was connected to an actuator using a thin wire. By setting the demonstrator on a slight incline, it could thus be actuated in both directions with negligible disturbance to the measurements.

Unless mentioned otherwise, all experiments are conducted using the EFH3 ferrofluid from Ferrotec.

3.2.1. Load and stiffness

The load and stiffness of the stage can determined by a compression test using a Zwick/Roell Z005 materials test frame. In this test the load–fly height curve can be generated. The load–fly height curve of a single bearing pad is measured using the same setup, in this case the head of the materials test frame is used as the bearing surface. The fly height is then defined as the distance between the magnet surface and the head of the materials test frame.

The stiffness of the stage can also be determined by adding a defined mass to the table while measuring the fly height of the table. This method, which requires less resources and is less time consuming, is used to gain an understanding of the influence of the increase of the individual fly heights.

By adding weight until the mover stops moving freely the load capacity can be determined easily. The free moving of the mover can be determined by placing the mover on a small incline (1 deg), and as the mover is released it should accelerate to a constant velocity. If this is not the case, contact between mover and base is present and thus the maximum load capacity is exceeded.

3.2.2. Trail formation

Fig. 6 shows the trail formation in the bearing. The trail thickness can be deduced from the colour of the trail. The light brown on the right and almost black on the left indicate a correlation between the amount of fluid loss and the movement velocity. The influence of this trail formation is experimentally determined by measuring the height of the stage before and after a stroke. This is done for different amounts of fluid in the system and for different translation speeds.

3.2.3. Evaporation

The evaporation rate of the ferrofluid was determined by placing five grams of fluid in a Petri dish. The fluid-air interface was 58 cm^2 and the temperature was kept between 18 and 22 degrees Celsius. The Petri dish with fluid have been weighed at a number of moments in time. The

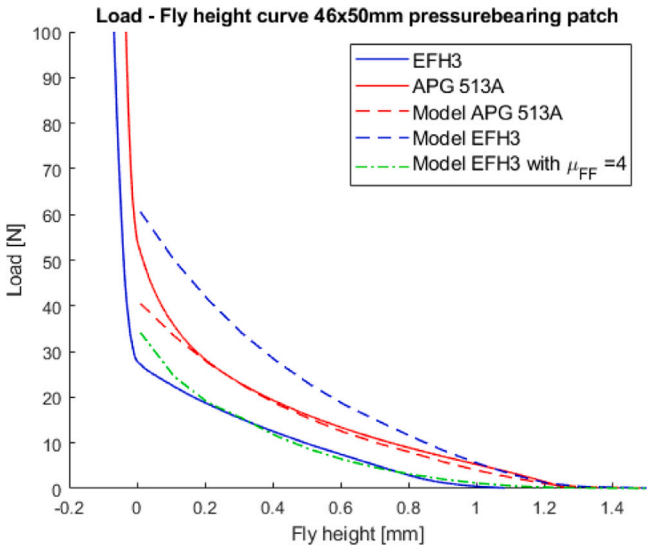

Fig. 7. Load–fly height curve of 23 × 1 pressure bearing pad with EFH3 and APG 513A ferrofluid.

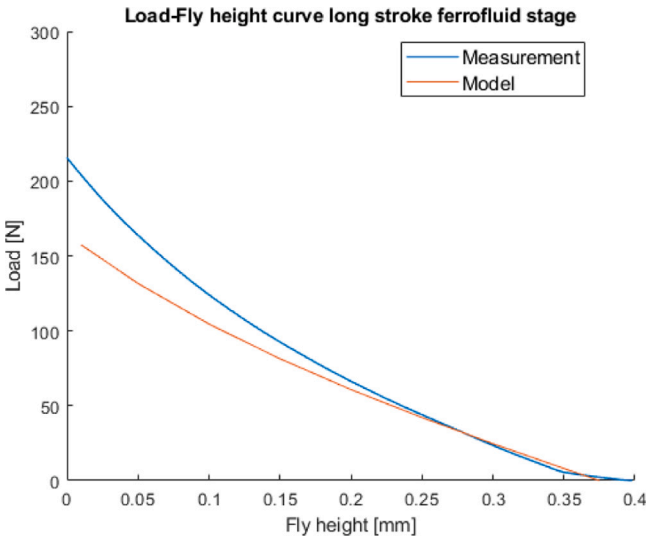

Fig. 8. Load–fly height curve of stage. The crosshead velocity of the materials test frame was set to 0.5 mm/min. The initial fly height without payload is 0.39 mm for the bottom bearing pad and 0.36 mm for the top bearing pad. The bearing pads are modelled with a relative permeability of 4 for the ferrofluid.

effects of evaporation on the fluid viscosity and magnetic properties are investigated using a rheometer (Anton Paar MCR302). This rheometer is capable of generating a magnetic field comparable to the field at the surface of the pressure bearing pads. The evaporation rate is established by measuring the mass loss of the Petri dish over time. Fluid samples with different percentages of mass loss are then evaluated using the rheometer. This same experiment is redone for fluid samples with the same percentage of mass loss, this time resupplied to the original mass by addition of paraffin oil.

3.2.4. Damping

The damping of the stage is evaluated by setting the stage on a defined incline. The external stage is used to pull the mover on the slope and to release it at the highest point. Gravity will accelerate the stage until it reaches terminal velocity, which is measured using the 200 mm laser distance sensor. This is repeated several times for a combination of three different inclinations and three different amounts of payload. As the weight of the stage is known, the driving force can be calculated. The viscous damping coefficient can then be determined using Eq. (3) in which c is the damping coefficient, m_{mover} the mass of the mover, g_0 is the standard gravity, Θ is the incline angle of the stage, and $U_{terminal}$ is the terminal velocity of the stage.

$$c = \frac{m_{mover} \cdot g \cdot \sin\Theta}{U_{terminal}} \tag{3}$$

4. Bearing design validation

4.1. Single pressure bearing pad

Fig. 7 shows the results of the testing of the individual pressure bearing pad. Zero displacement was taken to be the point at which the pressure plate touches the magnets in the measurement.

4.2. Demonstrator stage

4.2.1. Load capacity and stiffness

The experiment from Section 4.1 was repeated for the full stage. The result of this is shown in Fig. 8. The individual fly heights of the top and bottom pad are calculated such that the modelled load generated by the bottom pad is equal to the modelled load of the top pad combined with the gravity forces. This result in 0.39 mm for the bottom pad and 0.36 mm for the top pad. The larger fly height for the bottom pads is the result of the larger size of the bottom pads in comparison to the top pads.

Table 6
Measured and modelled stiffness of stage for different fly heights for the respective bottom bearing pad/top bearing pad.

Fly height	[mm]	0.3/0.25	0.4/0.35	0.55/0.50
Measured Stiffness	[N/μm]	0.7	0.4	0.3
Modelled Stiffness	[N/μm]	0.57	0.42	0.36

The maximum sustained load capacity was determined by adding mass to the stage whilst moving on a small incline and was found to be 140 N for a stroke of under 100 mm and 120 N for a full stroke.

The stiffness was also determined at different initial fly heights by using the laser displacement sensors and a weight of 3 kg. The model parameters were chosen to be the same as in Fig. 8. Table 6 shows the results of these measurements. It can be seen that the model corresponds well with the measurements at larger fly heights. When the fly height decreases, the model and measurement diverge.

4.2.2. Trail formation

Fig. 9 shows the relative height of the stage after translation with different velocities. A significant height drop at higher translation velocities using a limited amount of ferrofluid can be seen. Fig. 10 shows the relative height of the stage for 55 g of fluid and different payload amounts. It can be seen that the payload has no noticeable influence on the repeatability of the height. The zero in these figures is taken as the mean value of the fly height at 0.01 m/s. The initial fly height was set to 0.55 mm for the bottom pad and 0.50 mm for the top pad.

4.2.3. Evaporation

The evaporation measurement resulted in an evaporation rate in the initial 74 h of $9.0 \cdot 10^{-5}$ g/(cm^2 h) for the EFH3 fluid. The evaporation rate in the next 43 h was $5.6 \cdot 10^{-5}$ g/(cm^2 h). Using a rheometer, the properties of the ferrofluid were evaluated after being subjected to evaporation. This was done for the EFH3 fluid subjected for a 7.7% mass evaporation and for a 16.9% mass evaporation and can be seen in Figs. 11 and 12. Fig. 11 shows the viscosity in the ferrofluid as a function of the shear rate. Fig. 12 shows the normal force exerted on the rheometer by the ferrofluid.

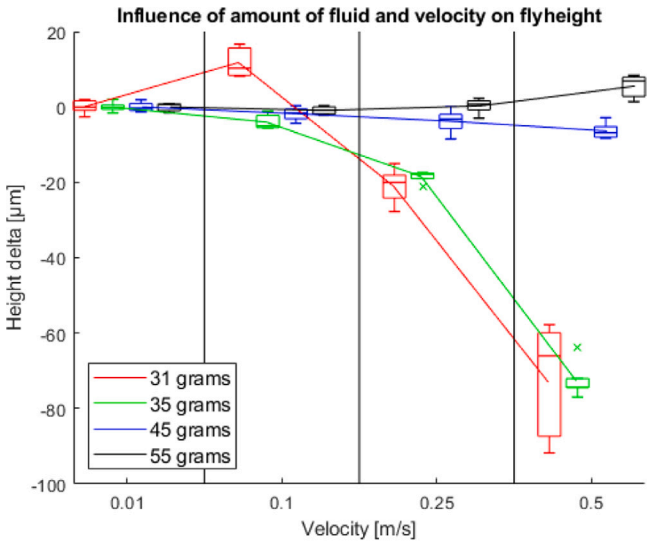

Fig. 9. Height delta of the mover height under translation at different speeds for different amounts of fluid. No payload was added to mover.

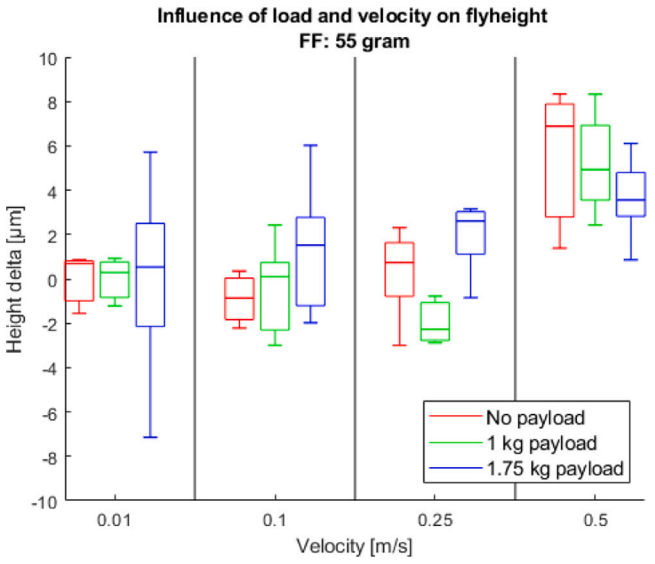

Fig. 10. Height delta of the mover height under translation at different speeds when filled with 55 g of FF.

4.2.4. Damping

The results of the damping experiment can be seen in Fig. 13, the stage was filled with 45 g of ferrofluid and has an unloaded fly height of 0.55 mm for the bottom pad and 0.50 mm for the top pad. A strong correlation between the damping coefficient, the load and velocity of the stage is present.

5. Discussion

5.1. Single pressure bearing pad

The data from the pressure bearing test using the APG 513A ferrofluid results in a load capacity of 40 N, resulting in 1.8 N/cm^2. The load capacity and stiffness of the bearing could have potentially been higher by selecting pocket bearings instead of pressure bearings. However, the values for load and stiffness are comparable to a previous implementation of a single pocket bearing stage [21] where a load capacity of 100 N was achieved using a surface area of 84 cm^2, resulting

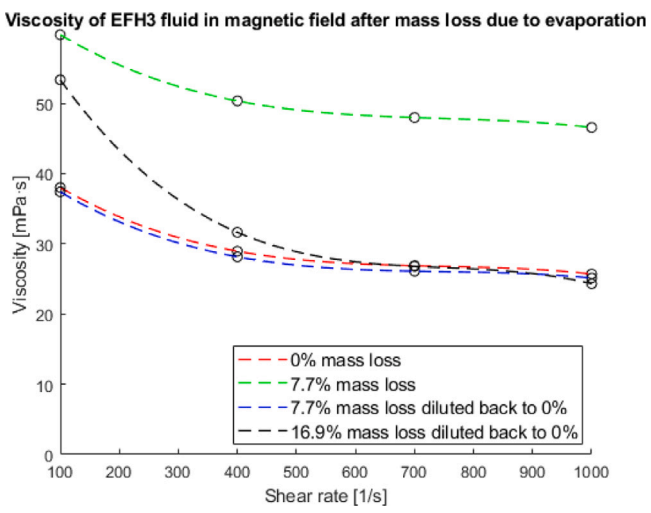

Fig. 11. Viscosity of EFH3 fluid for different levels of evaporation and dilution.

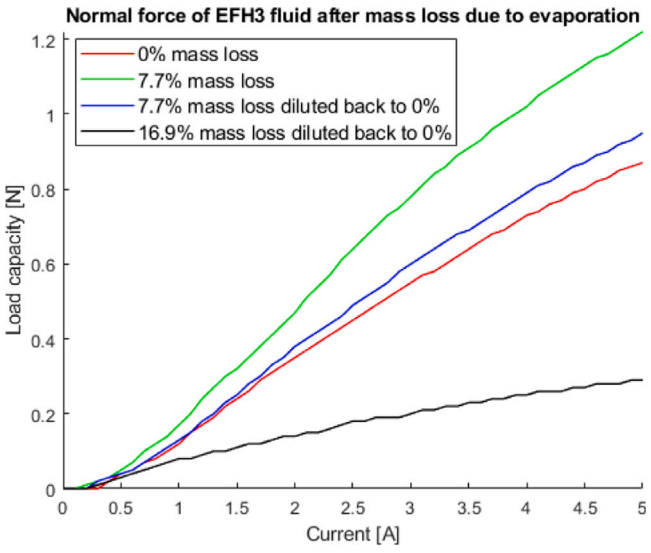

Fig. 12. Normal force exerted by EFH3 fluid on the rheometer for different levels of evaporation and dilution.

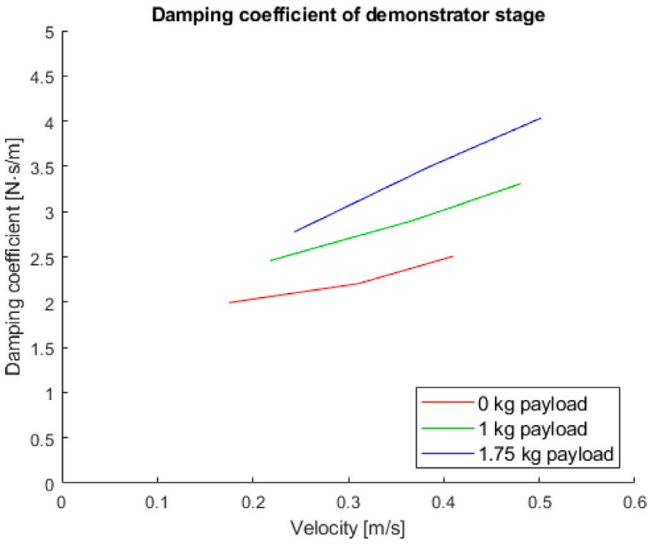

Fig. 13. Damping coefficient of demonstrator stage for different loads.

in 1.2 N/cm^2. Thus, to improve over the current design more complex pocket bearings with multiple seals would be required. This would result in more pockets of air which all need to be managed to maintain repeatability.

The load capacity using the EFH3 fluid is lower than with the APG 513A. This is unexpected as the EFH3 has a higher saturation magnetization. This behaviour might be explained by the loss of colloidal stability due to the high gradient in the magnetic field [43]. Magnetic particles will then accumulate at the corners of the magnets. This accumulation can be problematic in this specific magnet geometry as a large build-up of particles in between the two oppositely magnetized magnets will cause a short circuit in the magnetic field.

This behaviour is simulated in the model using an increase of relative permeability. A relative permeability of 4 is in close agreement with the measurement of the EFH3 fluid. This can be seen in Fig. 7.

5.2. Demonstrator stage

5.2.1. Load capacity & stiffness

The load–fly height curve shows that the behaviour of the stage is similar to the model at larger fly heights, and that the model and measurement diverge when the fly height of the stage approaches zero. This behaviour can be explained by squeeze film damping.

It can be seen that in the sense of load capacity, an ferrofluid stage can achieve a similar load capacity as a comparable aerostatic stage. The stiffness of the aerostatic stage however is several times higher. The high stiffness is required in the aerostatic stage to move resonance spikes from the underdamped eigenmodes to a frequency well above the desired bandwidth. As the ferrofluid stage uses a more viscous fluid, the eigenmodes are overdamped and thus much less of a problem. Thus, from a control point of view the stiffness does not necessarily need to be high. As the stiffness of the stage is known and stable under translation, it can easily be compensated for.

The specific trend in the relation between the load capacity and displacement can be attributed to the trail formation. As more ferrofluid is lost to the trail, the load capacity is diminished resulting in the mover running aground. The stiffness of the stage can be increased by decreasing the fly height of the top and bottom bearing pads. This can be done by decreasing the difference in height between mover and base. This way a stiffness of up to 0.7 N/μm can be achieved at a fly height of 0.3 mm and 0.25 mm for bottom and top bearing pads, respectively. The increase in stiffness comes at the cost of a reduction in load capacity. The fly height can be chosen based on the application, a larger fly height for applications requiring higher load capacity and a smaller fly height for applications requiring a higher stiffness.

The load capacity in lateral direction is not directly measured, but can be determined by using the bearing pad model. At a fly height of 1 mm this load capacity would be 80 N. When taking into account the fluid loss in translation, the effective lateral load capacity would be slightly lower. As the lateral pad is smaller and the reservoir in the mover remains equal in size, the drop in lateral load capacity is estimated to be less than 20 N, resulting in an estimated 60 N load capacity in lateral direction.

5.2.2. Trail formation

Fig. 9 shows that for a limited amount of ferrofluid, there is a significant drop in the height of the mover at higher translation velocities. The higher velocity induces more shear and as a result less fluid is present to support the load of the stage. Using a larger volume of ferrofluid eliminates this height drop, a height increase can even be observed in the height for an increase in pull back velocity. This height gain can partly be explained by the loss in fluid. The loss of 30 g of fluid would give an increase in fly height of 1 μm at a stiffness of 0.3 N/μm. A further explanation would be a difference in fluid loss and fluid supply in the top and bottom bearing pads. When the top pad has less fluid relatively to the bottom pad, the height of the mover will increase.

The increased stability in fly height can be explained by the reservoirs at the corners of the bearing pads as seen in Fig. 2. A larger volume of ferrofluid ensures there is an excess amount of fluid available on the mover to replace lost ferrofluid due to trail formation.

Fig. 10 shows the relative height of the mover for 55 g of fluid and different payload amounts. It can be seen that the payload has limited influence on the repeatability of the height of the mover. This figure shows the stage can accommodate a payload of 1 kg at a maximum velocity of 0.25 m/s with an out-of-plane height stability of ± 3 μm, and ± 7 μm for a payload of 1.75 kg at a maximum velocity of 0.5 m/s.

In past implementations of ferrofluid bearings into precision movement stages, the performance has been severely limited by trail formation. Typical values are that for a stroke of just several centimetres the loss of mover height is in the order of 1 μm/mm translation [21,23]. In comparison, both the attained stroke and stability of the mover height in the realized demonstrator stage are of exceptional performance.

5.2.3. Evaporation

Fig. 11 shows a severe increase in viscosity, both with and without magnetic field as a result of the evaporation of the carrier fluid. When the ferrofluid fluid is diluted back to the original mass by adding the required amount of carrier fluid, the viscosity of the fluid also reverts back to original. However, this was observed only up to a 7.7% evaporated fluid. A very probable explanation of this limit is the loss of colloidal stability of the fluid when evaporation exceed a certain value. Individual particles then agglomerate and no longer disperse when diluted back to original mass.

Fig. 12 shows the normal force exerted on the rheometer by the ferrofluid. This supports the theorized refilling of the carrier fluid for small levels of evaporation. Again, here can be seen that there is less normal force for the further evaporated fluid, which can also be caused by agglomerations in the fluid.

Due to the relatively large wetted surface area in the bearing, the overall mass loss due to evaporation using the EFH3 fluid will be in the order of magnitude of one percent per day. This means that after a week the viscosity in the fluid has doubled. After a few more days the fluid will lose colloidal stability and the individual particles will agglomerate. This process can be reversed by 'lubricating' the bearing occasionally through the addition of carrier fluid. The properties of the fluid will then return to their original specification. This has yet to be tested inside a working bearing system, however experiments using the rheometer look very promising.

Alternatively, a different solution to the evaporation problem would be the use of a ferrofluid with a very low vapour pressure. Where kerosene based EFH3 ferrofluid has a vapour pressure of 0.1 kPa [37], the vapour pressure of the H9-LT ferrofluid from Liquid-Research has a vapour pressure of $\sim 1 \cdot 10^{-7}$ kPa [44]. Based on the difference in vapour pressure the evaporation rate of the H9-LT ferrofluid will be several orders of magnitude lower than the evaporation rate of the EFH3 ferrofluid [45]. This would make a system to resupply evaporated carrier fluid unnecessary as the effects of evaporation will only be noticeable after several years. Low vapour pressure ferrofluids however are expensive and have a high viscosity. The H9-LT ferrofluid has a viscosity of 300 mPa s, which is 25 times higher than the used EFH3 ferrofluid. Primarily the high viscosity is problematic as it will increase damping and trail formation, thus reducing the possible stroke length and mover velocity.

5.2.4. Damping

The damping in the system is relatively constant and predictable, a function of movement velocity and payload. This makes open loop controlling a possibility in systems with lower positioning requirements. For high precision requirements, the damping attenuates high frequency noise and makes implementing of a (basic) PID controller possible [11]. The strong correlation of the damping coefficient indicates a velocity dependent flow profile in the ferrofluid.

Table 7
Comparison of specifications of aerostatic bearing stage and ferrofluid demonstrator stage.

	Unit	PI aerostatic bearing A-110.300	Ferrofluid demonstrator stage	Goal achieved
Travel	mm	300	460	✓
Maximum payload	N	100 normal	120 normal, 60 lateral	✓
Stiffness	N/μm	30-60 (estimated)	0.4	×
Moving mass	kg	2.6	1.8[a]	✓
Outer dimensions (W × L × H)	mm	160 × 575 × 60	180 × 600 × 80	✓[b]
Mover dimensions (W × L × H)	mm	160 × 200 × 60	139 × 124 × 60	✓
Straightness & Flatness	μm	< ± 1	< ± 8 (Fluid loss only)	×
Maximum velocity	m/s	1	–	?

[a]No actuation is added to the demonstrator stage at this stage.
[b]Outer dimensions of demonstrator can be reduced without loss of performance.

5.3. Comparison with aerostatic stage

The goal of this research was to demonstrate the possibility of a passive linear guide using ferrofluid pressure bearings capable of competing with an existing aerostatic stage. Table 7 shows the comparison between the realized demonstrator model and the PI linear stage with air bearings. It can be seen that the stage is only outperformed by the aerostatic bearing stage in terms of stiffness and straightness and the need for fluid management. The maximum velocity of the stage has yet to be determined.

6. Conclusion

In comparison to previous implementations of ferrofluid bearings, the realized stage greatly improves the stroke length and out-of-plane stability in mover height. However, the attained stability and stiffness is less than can be achieved in an aerostatic bearing stage. Thus, the use of this stage is not recommended in applications where these are critical, such as in sub-micrometre lithography stages. However, in comparison to aerostatic stages, the ferrofluid bearing can provide the same stick–slip free motion without the need for a constant supply of air or tight manufacturing tolerances. Moreover, the ferrofluid bearing approaches the same out-of-plane stability for a lower payload and velocity. The long term performance of the ferrofluid stage is dependent on the timely supply of carrier fluid. If resupply is not done before a certain amount of evaporation occurs, the magnetic properties of the ferrofluid are irreversibly lost. Overall, it can be concluded that, depending on the demands of the application, the ferrofluid bearing is a feasible alternative to aerostatic bearings.

From the findings in this research the following conclusions can be drawn:

- Optimized ferrofluid pressure bearings can compete with single seal pocket bearings,
- Magnets can be used in close proximity to conductors without significant eddy current damping by choosing the geometry and orientation of the magnets properly,
- The use of a reservoir on the mover results in a stable fly height under translation,
- The magnetic and viscous properties of ferrofluids subjected to moderate evaporation can be restored by resupplying the ferrofluid with carrier fluid,
- Timely resupply of carrier fluid is required to prevent irreversible loss of magnetic performance of the ferrofluid,
- The friction in the stage is only the result of viscous damping and is primarily affected by velocity and fly height,
- It is possible to design and manufacture a linear ferrofluid stage to specification.

Declaration of competing interest

The authors declare that they have no known competing financial interests or personal relationships that could have appeared to influence the work reported in this paper.

References

[1] Lentini L, Moradi M, Colombo F. A historical review of gas lubrication: From reynolds to active compensations. Tribol Ind 2018;40(2):165–82. http://dx.doi.org/10.24874/ti.2018.40.02.01.

[2] Tan KK, Huang S, Liang W, Yu S. Development for precise positioning of air bearing stages. In: 2012 IEEE international conference on mechatronics and automation, ICMA 2012. 2012, p. 1943–8. http://dx.doi.org/10.1109/ICMA.2012.6285119.

[3] Papell SS. Papell - 1965 - Low viscosity magnetic fluids obtained by the colloidal suspension of magnetic particles. 1965, US patent.

[4] Rosensweig R. Buoyancy and stable levitation of a magnetic body immersed in a magnetizable fluid. Nature 1966;210(5036):613–4. http://dx.doi.org/10.1038/210613a0.

[5] Rosensweig R. Bearing arrangement with magnetic fluid defining bearing pads. 1971.

[6] Van Beek A. Engineering design lifetime performance and reliability. Delft: TU Delft; 2012.

[7] Peijnenburg AT, Vermeulen JP, van Eijk J. Magnetic levitation systems compared to conventional bearing systems. Microelectron Eng 2006;83(4-9 SPEC. ISS.):1372–5. http://dx.doi.org/10.1016/j.mee.2006.01.248.

[8] Reck M. Air bearings : When to use and air bearings: When to use and when to avoid in your motion application.

[9] Boots A. Operational range of a ferrofluid pocket bearing (MSc Thesis), TU Delft; 2018.

[10] Brian Rowe W. Hydrostatic, aerostatic and hybrid bearing design. Hydrostatic, aerostatic and hybrid bearing design. Elsevier Inc.; 2012, http://dx.doi.org/10.1016/C2011-0-07331-3.

[11] Schmidt C, Heinzl J, Brandenburg G. Control approaches for high-precision machine tools with air bearings. IEEE Trans Ind Electron 1999;46(5):979–89. http://dx.doi.org/10.1109/41.793347.

[12] Dong Z, Liu P, Ding H. Kalman estimator-based state-feedback high-precision positioning control for a micro-scale air-bearing stage. In: Lecture notes in computer science (Including subseries lecture notes in artificial intelligence and lecture notes in bioinformatics). LNAI, vol. 5928, 2009, p. 765–75. http://dx.doi.org/10.1007/978-3-642-10817-4{_}76.

[13] Sorensen KL, Singhose W, Dickerson S. A controller enabling precise positioning and sway reduction in bridge and gantry cranes. Control Eng Pract 2007;15(7):825–37. http://dx.doi.org/10.1016/j.conengprac.2006.03.005.

[14] Fleming AJ, Aphale SS, Moheimani SO. A new robust damping and tracking controller for SPM positioning stages. In: Proceedings of the American control conference. 2009, p. 289–94. http://dx.doi.org/10.1109/ACC.2009.5159934.

[15] Sung E, Seo C-h, Song H, Choi B, Jeon Y, Choi Y-M, et al. Design and experiment of noncontact eddy current damping module in air bearing–guided linear motion system. Adv Mech Eng 2019;11(8):168781401987142. http://dx.doi.org/10.1177/1687814019871424, URL: http://journals.sagepub.com/doi/10.1177/1687814019871424.

[16] Tsumura T, Yoshioka H, Shinno H, Sawano H. Magnetically preloaded aerostatic guideway for high speed nanometer positioning. J Adv Mech Des Syst Manuf 2014;8(4):JAMDSM0054. http://dx.doi.org/10.1299/jamdsm.2014jamdsm0054, URL: http://jlc.jst.go.jp/DN/JST.JSTAGE/jamdsm/2014jamdsm0054?lang=en&from=CrossRef&type=abstract.

[17] Café M, Spronck J. Nanometer precision six degree s of freedom planar motion stage with ferrofluid bearings. In: DSPE conference on precision mechatronics. 2014, p. 43–6.

[18] Café M. Nanometer precision six degrees of freedom planar motion stage with ferrofluid bearings. Technical Report, TU Delft; 2014.

[19] Mok G. The design of a planar precision stage using cost effective optical mouse sensors (MSc Thesis), TU Delft; 2015.

[20] Alvarez-Aguirre A, Mok G, HosseinNia SH, Spronck J. Performance improvement of optical mouse sensors: Application in a precision planar stage. In: 2016 international conference on manipulation, automation and robotics at small scales, MARSS 2016. 2016, http://dx.doi.org/10.1109/MARSS.2016.7561698.

[21] van Moorsel L. A planar precision stage using a single image sensor (MSc Thesis), TU Delft; 2017.
[22] Uhlmann E, Bayat N. High precision positioning with ferrofluids as an active medium. CIRP Ann - Manuf Technol 2006;55(1):415–8. http://dx.doi.org/10.1016/S0007-8506(07)60448-X.
[23] van Veen S. Planar ferrofluid bearings (MSc Thesis), TU Delft; 2013.
[24] Deng R, Van Veen S, Café M, Spronck JW, Munnig Schmidt RH. Linear nano-positioning stage using ferrofluid bearings. In: Conference proceedings - 14th international conference of the european society for precision engineering and nanotechnology, EUSPEN 2014, Vol. 1. 2014, p. 372–5, URL: https://news.microsoft.com/apac/features/putting-digital-transformation-on-the-business-agenda/.
[25] Assadsangabi B, Tee MH, Takahata K. Ferrofluid-assisted levitation mechanism for micromotor applications. In: 2013 transducers and eurosensors XXVII: The 17th international conference on solid-state sensors, actuators and microsystems, TRANSDUCERS and EUROSENSORS 2013, Vol. 17. 2013, p. 2720–3. http://dx.doi.org/10.1109/Transducers.2013.6627368.
[26] Osman TA, Nada GS, Safar ZS. Static and dynamic characteristics of magnetized journal bearings lubricated with ferrofluid. Tribol Int 2001;34(6):369–80. http://dx.doi.org/10.1016/S0301-679X(01)00017-2.
[27] Ravaud R, Lemarquand G, Lemarquand V. Mechanical properties of ferrofluid applications: Centering effect and capacity of a seal. Tribol Int 2010;43(1–2):76–82. http://dx.doi.org/10.1016/j.triboint.2009.04.050.
[28] Odenbach S. Colloidal Magnetic Fluids. Lecture notes in physics, vol. 763, Berlin, Heidelberg: Springer Berlin Heidelberg; 2009, p. 430. http://dx.doi.org/10.1007/978-3-540-85387-9, URL: http://link.springer.com/10.1007/978-3-540-85387-9.
[29] Wang Z, Hu Z, Huang W, Wang X. Elastic support of magnetic fluids bearing. J Phys D: Appl Phys 2017;50(43). http://dx.doi.org/10.1088/1361-6463/aa86f9.
[30] Boots AS, Krijgsman LE, de Ruiter BJ, Lampaert SG, Spronck JW. Increasing the load capacity of planar ferrofluid bearings by the addition of ferromagnetic material. Tribol Int 2019;129(May 2018):46–54. http://dx.doi.org/10.1016/j.triboint.2018.07.048.
[31] Lampaert SG, Fellinger BJ, Spronck JW, van Ostayen RA. In-plane friction behaviour of a ferrofluid bearing. Precis Eng 2018;54(May):163–70. http://dx.doi.org/10.1016/j.precisioneng.2018.05.013.
[32] Lampaert SG, Spronck JW, van Ostayen RA. Load and stiffness of a planar ferrofluid pocket bearing. Proc Inst Mech Eng J 2018;232(1):14–25. http://dx.doi.org/10.1177/1350650117739200.
[33] Lampaert S. Planar ferrofluid bearings modelling and design principles (MSc Thesis), 2015.
[34] Physik Instrumente. PIglide air bearing technology datasheet. Physik Instrumente (PI) GmbH & Co.; 2019.
[35] HKCM Engineering eK. Magnet-cuboid Q50x02x02Ni-N35. 2019, URL: https://www.hkcm.de/HKCM_allinone.php?l=&id=53809&tolerance=1&force=1&flux=1&coating=1&bh=1&l=en.
[36] van den Toorn SWM. Ferrofluid linear long stroke stage (MSc Thesis), 2020.
[37] Ferrotec. Ferrofluid data sheet EFH series. 2011.
[38] COMSOL AB. COMSOL multiphysics 5.4. Stockholm, Sweden: COMSOL AB; 2019, URL: www.comsol.com.
[39] The Mathworks Inc. Matlab R2018b. Natick, Massachusetts: The Mathworks Inc.; 2018.
[40] Odenbach S. Recent progress in magnetic fluid research. J Phys Condens Matter 2004;16(32). http://dx.doi.org/10.1088/0953-8984/16/32/R02.
[41] Ferrotec. Data sheet APG 2100 series. 2013.
[42] Micro-Epsilon, Datasheet optoNCDT 1420. URL: https://www.micro-epsilon.com/download/products/cat--capaNCDT--en.pdf.
[43] Moeser GD, Roach KA, Green WH, Alan Hatton T, Laibinis PE. High-gradient magnetic separation of coated magnetic nanoparticles. AIChE J 2004;50(11):2835–48. http://dx.doi.org/10.1002/aic.10270, URL: http://doi.wiley.com/10.1002/aic.10270.
[44] Liquids Research Ltd., Ferrofluids for sealing applications SI. URL: https://www.liquidsresearch.co.uk/en-GB/for_sealing_applications_si-61.aspx.
[45] Mackay D, Van Wesenbeeck I. Correlation of chemical evaporation rate with vapor pressure. Environ Sci Technol 2014;48:10259–63. http://dx.doi.org/10.1021/es5029074, URL: https://pubs.acs.org/sharingguidelines.